Оригинальные статьи

Original papers

УДК 541.138:546.24:546.87

BISMUTH AND LEAD UNDERPOTENTIAL DEPOSITION ON BISMUTH TELLURIDE: NEW INSIGHTS INTO THE ELECTROCHEMICAL SYNTHESIS OF BISMUTH TELLURIDE AND EVALUATION OF REAL SURFACE AREA

***A. S. BAKAVETS*[a], *Y. M. ANISKEVICH*[a], *G. A. RAGOISHA*[b], *E. A. STRELTSOV*[a]**

[a]*Belarusian State University, Niezaliežnasci Avenue, 4, 220030, Minsk, Belarus*
[b]*Institute for Physical Chemical Problems of the Belarusian State University, Lieninhradskaja Street, 14, 220006, Minsk, Belarus*

Corresponding author: G. A. Ragoisha (ragoishag@bsu.by)

The underpotential deposition (UPD) processes of lead and bismuth on bismuth telluride (Bi_2Te_3) have been discovered with the underpotential shifts 0.3 V for Pb UPD and 0.1 V for Bi UPD. The Pb UPD was shown to be helpful for bismuth telluride real surface area evaluation. Potentiodynamic profiles of Pb UPD differ significantly on bismuth telluride and tellurium substrates, which helps to control purity of bismuth telluride electrodeposit. Bismuth telluride films were deposited from acidic solution of TeO_2 and bismuth salt on steel substrates using potential pulse electrodeposition and cyclic voltammetry (CV). The CV has proved that the stoichiometric bismuth telluride deposition proceeds in the potential range of metallic bismuth anodic oxidation, which excludes metallic Bi as a required intermediate in the sustained electrodeposition of Bi_2Te_3. Bismuth adatoms are much more stable than metallic (bulk) Bi^0 on Bi_2Te_3 and they are very likely to be involved in the electrodeposition mechanism. The potentials of pulsed electrodeposition were optimized taking into account the UPD of Bi. The absence of Te and Bi phases in electrodeposited Bi_2Te_3 was proved by XRD and CV.

Образец цитирования:
Боковец А. С., Анискевич Е. Н., Рагойша Г. А., Стрельцов Е. А. Подпотенциальное осаждение висмута и свинца на теллуриде висмута: новое понимание электрохимического синтеза теллурида висмута и оценки реальной площади поверхности // Журн. Белорус. гос. ун-та. Химия. 2017. № 2. С. 3–13 (на англ.).

For citation:
Bakavets A. S., Aniskevich Y. M., Ragoisha G. A., Streltsov E. A. Bismuth and lead underpotential deposition on bismuth telluride: new insights into the electrochemical synthesis of bismuth telluride and evaluation of real surface area. *J. Belarus. State Univ. Chem.* 2017. No. 2. P. 3–13.

Авторы:
Алексей Степанович Боковец – студент химического факультета. Научный руководитель – Г. А. Рагойша.
Евгений Николаевич Анискевич – студент химического факультета. Научные руководители – Е. А. Стрельцов, Г. А. Рагойша.
Геннадий Антонович Рагойша – кандидат химических наук, доцент; ведущий научный сотрудник.
Евгений Анатольевич Стрельцов – доктор химических наук, профессор; заведующий кафедрой электрохимии химического факультета.

Authors:
Aliaksei Bakavets, student at the faculty of chemistry.
alexeibokovets@gmail.com
Yauhen Aniskevich, student at the faculty of chemistry.
aniskevich.y.m@gmail.com
Genady Ragoisha, PhD (chemistry), docent; leading researcher.
ragoishag@bsu.by
Eugene Streltsov, doctor of science (chemistry), full professor; head of the department of electrochemistry, faculty of chemistry.
streltea@bsu.by

The third form of Bi^0 with oxidation potential intermediate between those of bulk Bi^0 (first form) and Bi adlayer (second form) has been discovered in the electrodeposition with the excess of Bi^{3+} in electrolyte and attributed to Bi atoms intercalated in Van der Waals planes of bismuth telluride. The effect of Bi intercalation is of interest as a means of loosening the interlayer interactions in the layered structure of bismuth telluride for its further application in exfoliation procedures.

Key words: bismuth telluride; electrodeposition; underpotential deposition; UPD.

ПОДПОТЕНЦИАЛЬНОЕ ОСАЖДЕНИЕ ВИСМУТА И СВИНЦА НА ТЕЛЛУРИДЕ ВИСМУТА: НОВОЕ ПОНИМАНИЕ ЭЛЕКТРОХИМИЧЕСКОГО СИНТЕЗА ТЕЛЛУРИДА ВИСМУТА И ОЦЕНКИ РЕАЛЬНОЙ ПЛОЩАДИ ПОВЕРХНОСТИ

А. С. БОКОВЕЦ [1)]***, Е. Н. АНИСКЕВИЧ*** [1)]***, Г. А. РАГОЙША*** [2)]***, Е. А. СТРЕЛЬЦОВ*** [1)]

[1)] *Белорусский государственный университет, пр. Независимости, 4, 220030, г. Минск, Беларусь*
[2)] *Учреждение БГУ «Научно-исследовательский институт физико-химических проблем», ул. Ленинградская, 14, 220006, г. Минск, Беларусь*

Обнаружено явление подпотенциального осаждения (UPD) свинца и висмута на теллуриде висмута (Bi_2Te_3) со значениями подпотенциального сдвига 0,3 и 0,1 В соответственно. UPD свинца позволяет определять реальную площадь поверхности теллурида висмута. Потенциодинамический профиль UPD Pb значительно отличается на теллуриде висмута и теллуре, что можно использовать для оценки чистоты электроосаждаемого теллурида висмута. Теллурид висмута осаждали из азотнокислого раствора TeO_2 и соли висмута на стальные подложки, используя импульсное осаждение и циклическую вольтамперометрию (ЦВА). Результаты ЦВА свидетельствуют о формировании теллурида висмута в том же интервале потенциалов, где происходит анодное окисление висмута, что исключает формирование металлического Bi^0 в качестве интермедиата осаждения Bi_2Te_3. Адатомы висмута более стабильны, чем металлический (массивный) Bi^0 на теллуриде висмута, в связи с чем вероятно их участие в электроосаждении теллурида висмута. Потенциалы импульсного осаждения оптимизировали, учитывая процесс UPD висмута. Отсутствие фаз Te и Bi в электроосажденном Bi_2Te_3 было подтверждено путем использования рентгенофазового анализа и ЦВА. Электроосаждение из растворов с избыточным содержанием Bi^{3+} в электролите выявило формирование третьей формы Bi^0, характеризуемой промежуточным значением потенциала окисления между массивным Bi^0 (первая форма) и адатомами Bi (вторая форма), которая может соответствовать атомам висмута, интеркалированным в плоскости Ван-дер-Ваальса теллурида висмута. Интеркаляция Bi может быть интересна как потенциальное средство для расслоения слоистой структуры теллурида висмута.

Ключевые слова: теллурид висмута; электроосаждение; подпотенциальное осаждение; UPD.

Introduction

Bismuth telluride Bi_2Te_3 is one of the most promising thermoelectric materials [1]. Thermoelectric devices convert temperature difference to voltage (Seebeck effect), or transfer heat from one side of the device to the other, thus producing spatially separated cooling and heating by the applied voltage (Peltier effect). The operation of thermoelectric device involves no movable actuating parts. This remarkable advantage of the thermoelectric coolers over conventional refrigerators enables production of highly durable and energy efficient heat sinks which can be easily built into various instruments. The potential of a thermoelectric material application depends on its «figure of merit» *ZT*; the latter approaches 1.0 for the advanced materials on the market and has to be further doubled to expand fundamentally the application areas.

$$ZT = \alpha^2 \sigma T / \kappa,$$

where α is the Seebeck coefficient; σ is electrical conductivity; T is absolute temperature; κ is the sum of electronic and lattice contributions to the total thermal conductivity. The thermoelectric parameters are intimately interrelated via carrier concentration, which makes the improvement of *ZT* to be a large challenge to the materials science. Two main strategies have been adopted to improve *ZT*. One is to maximize $\alpha^2\sigma$ through semiconductor energy band engineering. The other is to reduce the thermal conductivity. The reduction of κ is normally coupled with the reduction of σ; therefore nontrivial methods of thermal conductivity control are required. Nanostructuring and heterostructuring of Bi_2Te_3 with tellurides of other metals are the basic routes in the second strategy [2]. Both strategies critically depend on methods of controllable growth of heterostructures of bismuth telluride with tellurides or selenides of other metals.

Electrodeposition is one of the most efficient means to progress in the thermoelectric heterostructure synthesis for several reasons. First, the electrodeposition gives a great variety of semiconductor materials and nanostructures at room or moderately elevated temperature. Unlike the trivial control of a reaction by temperature which affects the whole system, the electrode potential controls the reaction by affecting just the electron subsystem, which provides diverse redox transformations in mild conditions without heating the object. Advanced methods combine application of different potentials in a single electrodeposition procedure to control deposit composition and morphology [3; 4]. Second, the electrochemical route of telluride synthesis can favour from the unique opportunity of nanoengineering on the atomic scale through UPD of atomic layers of metals and chalcogens [5–9]. The UPD is the deposition of adatoms and adlayers above the corresponding reversible potential of the electrodeposition of the same metal (or nonmetal) as bulk material. Nanoengineering of layered structures through electrochemically generated atomic layers is of special interest due to theoretical prediction of high *ZT* in quantum confined 2D quantum well systems [10]. The decoupling of thermal and electric conductivity in 2D quantum confined Bi_2Te_3-based heterostructures can result from the enhanced phonon scattering at heterointerfaces. This kind of layered systems is also becoming a hot topic in investigations of topological insulators [11; 12]. Third, the electrodeposition can proceed on electrodes with complex shape and can be combined with electrochemical assembly of heterostructures, so the preparation of a complex semiconductor thermoelectric material can be arranged in a single electrochemical procedure.

The UPD of bismuth [13–16] and tellurium [8; 17; 18] on metals, as well as bismuth UPD on tellurium [19] were extensively investigated, but the UPD of metals on bismuth telluride needed clarification, as well as the possible role of Bi UPD on Bi_2Te_3 in the electrodeposition of bismuth telluride. Underpotential deposition of lead on bismuth telluride was expected to proceed similar to Pb UPD on PbTe [20], and the electrochemically controllable deposition of Pb atomic layer on the tellurides is of interest as a route to preparation of Pb-containing chalcogenide quantum-dot superlattices which were shown to give *ZT* up to 1.6 [21].

The UPD is also the most efficient means of the real surface area measurement of metal [22] and metal chalcogenide [23] electrodes. The surface area is an important parameter which controls thermoelectric properties jointly with the composition and structure. In this work we used the discovered UPD of lead on bismuth telluride electrodes to evaluate their real surface area, which was required for comparing electrochemical activity of electrodes with different surface topology. Underpotential deposition and also intercalation of metals into bismuth telluride is also of interest in view of the search of exfoliation routes [24] to produce low-dimensional structures from bulk layered chalcogenides, e. g. lithium intercalation can cause exfoliation of layered chalcogenide materials [25; 26]. Our results obtained in this work suggest another way for possible separation of layered fragments of bismuth telluride – introduction of a metal into the layered structure already in the course of electrodeposition. The discrimination of metal adlayers located on the outer surface of a crystal from atoms of the same metal located in Van der Waals planes inside the crystal is required to progress in the electrochemical investigation of intercalation and exfoliation. We have found that electrochemical characterization was powerful enough to distinguish at least three forms of bismuth which were observed during bismuth telluride electrodeposition – bismuth as a separate phase, bismuth adlayer on bismuth telluride, and the third form with oxidation potential intermediate between the one of metallic Bi and Bi adlayer. Unlike bismuth adlayer which was limited in amount by the surface area, the third form which was attributed to bismuth located in Van der Waals planes inside the crystal can be generated in much higher amount at certain electrodeposition conditions.

Experimental

Stainless steel electrodes were used as conducting substrates for bismuth telluride electrodeposition and subsequent UPD of bismuth and tellurium on the electrodeposited bismuth telluride. The advantage of stainless steel over gold and platinum which are more commonly used in investigations of electrodeposition mechanisms results from its inability to stabilize adlayers of bismuth and tellurium, so the UPD of Bi and Te did not proceed on bare support and did not hide the processes related to bismuth telluride. Stainless steel has been already used in the investigation of Bi_2Te_3 electrodeposition mechanisms [27], but the authors of [27] did not distinguish various forms of Bi in Bi_2Te_3 and on Bi_2Te_3; therefore their conclusion of bismuth telluride electrodeposition proceeding via bismuth electrodeposition was inexact. In fact, the electrodeposition of stoichiometric Bi_2Te_3 proceeds in the potential range of metallic bismuth anodic oxidation, so metallic bismuth can hardly be a required intermediate of Bi_2Te_3 electrodeposition, though the deposition of Bi_2Te_3 is often accompanied by the deposition of metallic bismuth, when the process is conducted in the potential range of the both processes for higher deposition rate.

In this work, pulsed potentiostatic electrodeposition was used to deposit stoichiometric Bi_2Te_3 at acceptable deposition rate. The potential of the electrode was first kept in the range of Bi_2Te_3 deposition slightly above the potential of bismuth bulk phase formation for 100 ms with the subsequent switching for 900 ms at 1 Hz

frequency into the higher potential region just above the anodic peak of Bi oxidation, where the metallic bismuth was thermodynamically unstable and the stationary Bi_2Te_3 deposition rate approached zero. The lower and upper potentials in the pulses depended on the electrolyte composition and were 40 and 180 mV for the deposition from the solution with 2 : 3 Bi : Te atomic ratio. All potentials are presented vs. Ag/AgCl reference electrode with saturated KCl solution, the latter was separated from working solutions by salt bridge with glass tap.

Stainless steel electrodes were etched in concentrated nitric acid and polished by 1.0 and 0.05 μm alumina in series. The working part of the electrode (from 15 to 25 mm^2) was afterwards separated from the rest of the electrode by covering the latter with water resistant varnish, this procedure helped to control the surface area and the uniformity of electrodeposition conditions on the working part of the electrode surface. Finally, the electrode was subjected to 10 potential cycles between –0.4 and 0.8 V at 50 $mV \cdot s^{-1}$ in 3 mol/L nitric acid to provide reproducible electrochemical behaviour in the further electrodeposition experiments. The electrodeposition was performed in three-electrode electrochemical cell with Pt counter electrode. All electrolyte solutions were deaerated with nitrogen.

Gamry series G300 potentiostat was used in pulsed potentiostatic and cyclic voltammetry (CV) experiments. Potentiodynamic electrochemical impedance spectra (PDEIS) were obtained with a home built spectrometer [28; 15]. PDEIS spectra were analysed by methods discussed in [29; 30]. Empyrean X-ray diffractometer (PANalytical, Netherlands) was used for structural characterization of Bi_2Te_3. The XRD analysis was combined with energy dispersive X-ray spectroscopy to prove the deposit composition, as the similarity of the most intensive diffraction peaks of Bi_2Te_3 and Te complicated their accurate distinguishability by the mere XRD, especially in early stages of the electrodeposition when X-ray diffraction was dependent on the deposit particle sizes.

Results and Discussion

Figure 1 shows the CV data for Bi, Te and Bi_2Te_3 electrodeposition on steel. All three electrodeposition processes proceed with high nucleation overpotentials, and the overpotentials decrease strongly in the reverse scan and in subsequent potential cycles. Initially, the overpotential of tellurium nucleation on steel is much higher than that of bismuth nucleation, so the initiation of Bi_2Te_3 via bismuth electrodeposition suggested in [27] appears to be probable; however, the relative rates of Bi and Te deposition invert already in the reverse scan of the first CV cycle. After initiation, tellurium deposition becomes possible even in the potential region of metallic bismuth anodic oxidation (fig. 1, *a*) and the deposition of tellurium keeps preference over bismuth deposition during sustained cycling at equimolar concentrations of the electrolytes (fig. 1, *b*) and at Bi : Te atomic ratio that corresponds to Bi_2Te_3 stoichiometry (fig. 2). The anodic oxidation of Bi_2Te_3 shows up in the anodic scan 0.1 V before tellurium anodic oxidation (fig. 1 and 2). The important conclusion which follows from fig. 1 and 2 is that Bi_2Te_3 electrodeposition continues above the anodic oxidation peak of metallic bismuth. This is especially evident when comparing the CV obtained at «stoichiometric» Bi : Te atomic ratio in the solution (fig. 2). Thus, bulk bismuth nucleation is not required in the sustained electrodeposition of Bi_2Te_3.

The pulsed potentiostatic electrodeposition combines the high rate of the cathodic reaction in the low-potential phase of the applied rectangular periodic waveform with the stay above the oxidation peak of metallic bismuth which helps to keep the stoichiometric composition of the deposit. The lower limit of the periodic waveform was chosen so that the potential was sufficient to boost the initially small cathodic current in subsequent pulses as shown in inset to fig. 1, *a*. Much smaller anodic current which also increases in the initial stage of the pulsed deposition provides removal of superfluous bismuth and keeps compact the structure of the deposit.

Figure 3 shows the X-ray diffractogram of thus deposited Bi_2Te_3 in comparison with XRD of tellurium [31]. Both materials give few similar intensive diffraction peaks. XRD discriminates them reliably only at sufficiently high amount of the deposit, when the less intensive peaks can be compared.

Figure 4 presents a rather compact structure of the pulsed deposited Bi_2Te_3 by SEM images.

The increase above Bi : Te «stoichiometric» atomic ratio in the solution resulted in the additional wide anodic peak at 0.2 V, i. e. approximation 0.2 V above the potential of bulk bismuth anodic oxidation (fig. 5, *a*). The effect of the continuous cycling in that solution avoiding bismuth telluride oxidation is shown in fig. 5, *b*.

The anodic peak A_1 increases with a shift to lower potential and finally transforms into anodic peak A_2. The cathodic peak C_1 which is formed in the second cycle increases slowly in subsequent cycles and attains regular shape. Also a new cathodic peak C_2 grows with the cycling. When the reversal potential in the cycling is shifted to the potential of the cathodic current minimum between C_1 and C_2 (approximation 0 V), the CV shows the cathodic peak in the range of C_2 and the anodic peak in the range of A_1 but with a smaller current than the original A_1 (inset in fig. 5, *b*). The peak currents in the latter range have shown no evolution, when

the reversal potential was kept positive to the potential range of the cathodic peak C_1. The cathodic and anodic peaks shown in the inset in fig. 5, *b*, gave a hint of a surface limited reaction contributing to the electrodeposition of bismuth telluride, presumably bismuth underpotential deposition. In order to check the bismuth telluride capability of taking up metal adlayers above Nernst potential, we have examined the early stages of bismuth and lead cathodic deposition from solutions of their salts in the absence of TeO_2.

Figure 6 shows the two-stage cathodic reduction and anodic oxidation of lead on the pulsed deposited Bi_2Te_3. The potential of the left pair of cathodic and anodic peaks corresponds to the reversible Nernst potential of metallic Pb $E(Pb^{2+}/Pb_{bulk})$, while the pair of peaks at much higher potential reveals the underpotential deposition of Pb adlayer and its anodic oxidation.

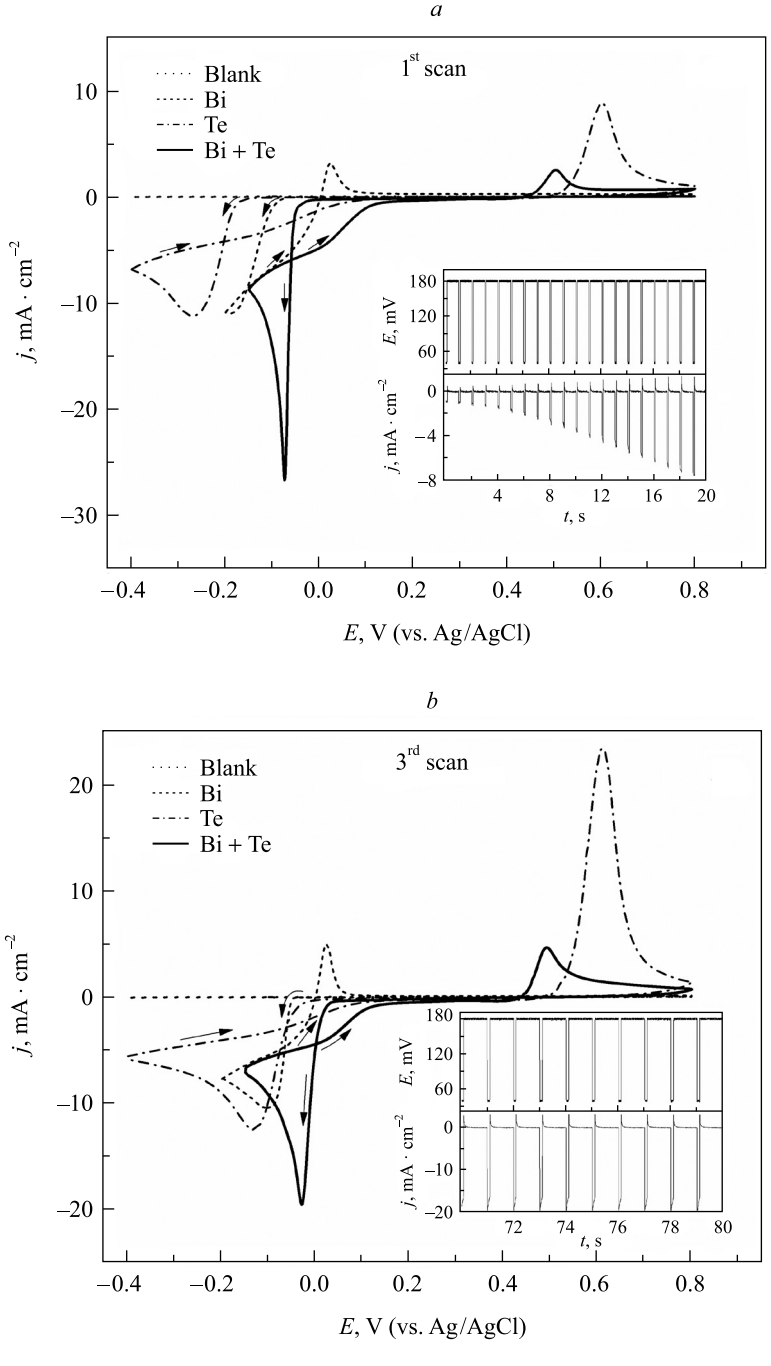

Fig. 1. Cyclic voltammograms of steel electrode in 12 mmol/L $Bi(NO_3)_3$ plus 18 mmol/L TeO_2 (solid), 30 mmol/L TeO_2 (dash-dotted), and 30 mmol/L $Bi(NO_3)_3$ (dashed) with 3 mol/L HNO_3 supporting electrolyte: *a* – first cycle; *b* – third cycle, $dE/dt = 50$ mV · s^{-1}. Dotted curve corresponds to 3 mol/L HNO_3 electrolyte (blank). Insets show the potential and current profiles in the beginning and in the sustained state of Bi_2Te_3 pulsed electrodeposition

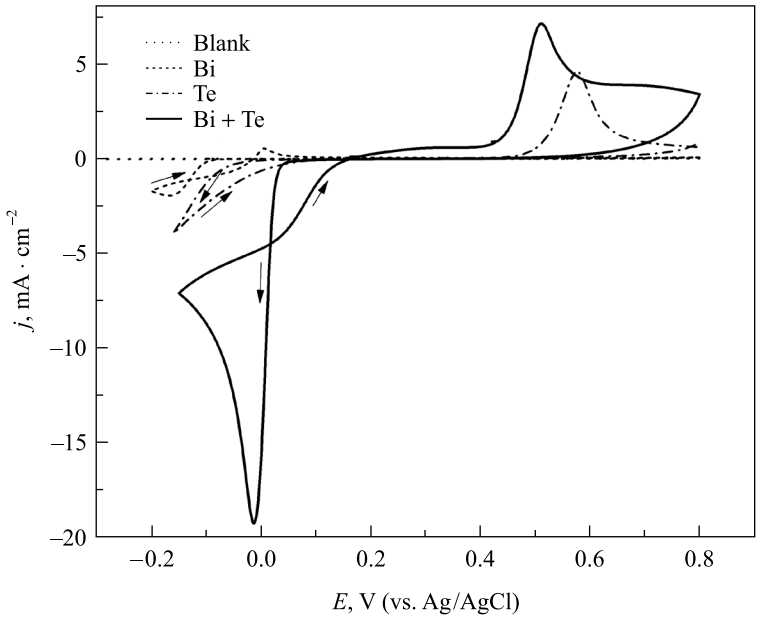

Fig. 2. Cyclic voltammograms of steel electrode in 12 mmol/L $Bi(NO_3)_3$ plus 18 mmol/L TeO_2 (solid), 18 mmol/L TeO_2 (dash-dotted), and 12 mmol/L $Bi(NO_3)_3$ (dashed) with 3 mol/L HNO_3 supporting electrolyte. $dE/dt = 50$ mV · s^{-1}. Dotted curve corresponds to 3 mol/L HNO_3 electrolyte (blank)

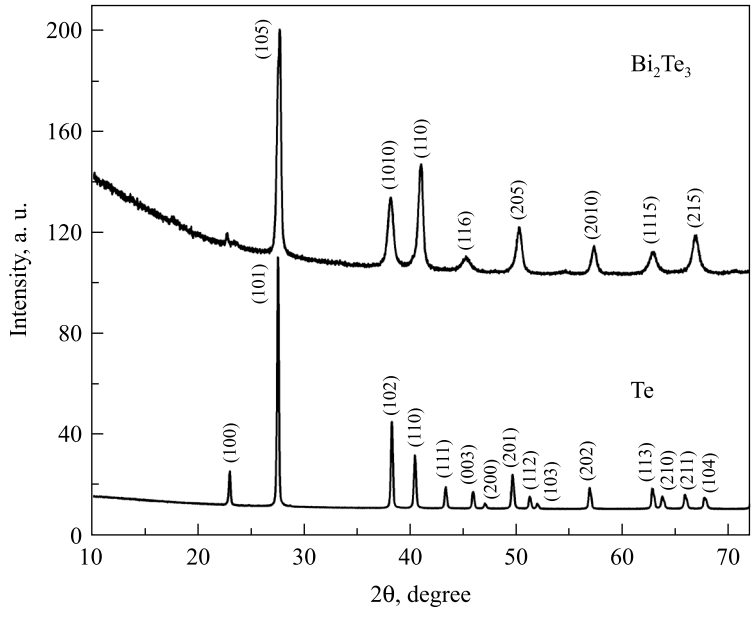

Fig. 3. XRD of the pulsed electrodeposited Bi_2Te_3 (detached from the substrate) and of chemically deposited tellurium

The UPD of lead on bismuth telluride shows much similarity with lead underpotential deposition processes on lead telluride [20] and on tellurium [20; 8]. Figure 7, *a*, compares Pb UPD on Bi_2Te_3 with the UPD on tellurium at sustained cycling. The two-humped cathodic peak in lead UPD on tellurium results from superposition of Pb UPD on Te (the left hump of the peak) and Pb UPD on PbTe inclusions that are formed by Pb adatoms interaction with tellurium at prolonged cycling (the right hump of the peak) [20]. Lead UPD proceeds on bismuth telluride in the intermediate potential range between the two UPD processes. The regular shape of the cathodic peak of Pb UPD on Bi_2Te_3 is the indication of Bi_2Te_3 purity (the deposit contains no elementary tellurium).

The potentials of Pb adlayer cathodic deposition on Bi_2Te_3 and anodic stripping from Bi_2Te_3 are a little bit lower than those of Pb_{ad} on PbTe, which is the indication of a slightly weaker Pb_{ad} – Bi_2Te_3 interaction compared to that of Pb_{ad} – PbTe. The cathodic and anodic peaks in Pb UPD on Bi_2Te_3 do not overlap, which

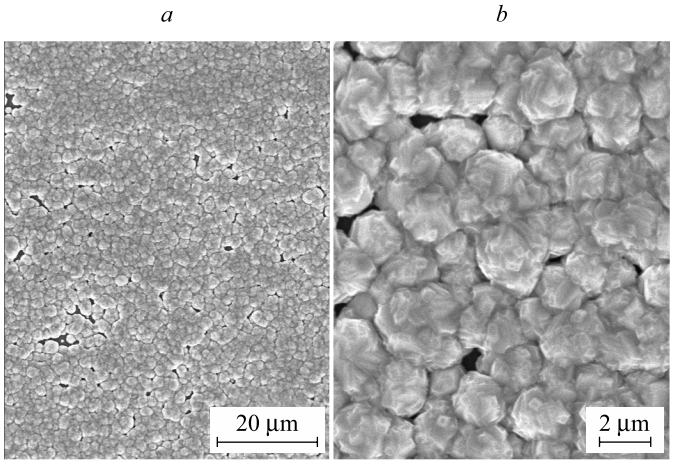

Fig. 4. SEM image of Bi_2Te_3 obtained by pulsed electrodepositon on steel

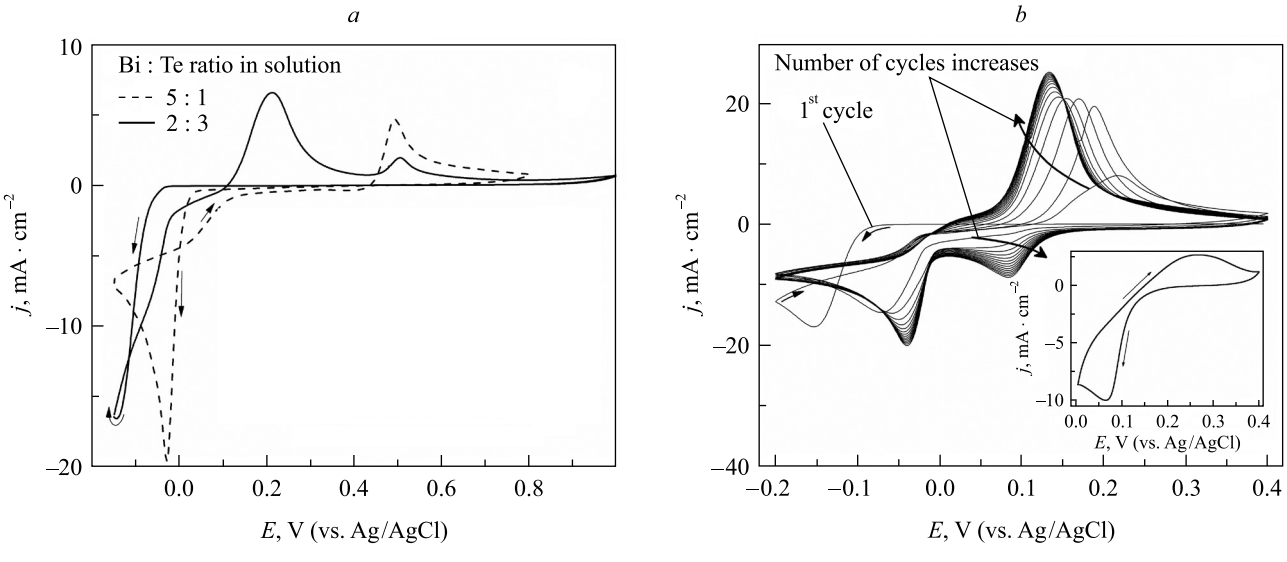

Fig. 5. Cyclic voltammograms of steel electrode in the electrolytes with different Bi : Te ratio:
12 mmol/L $Bi(NO_3)_3$ plus 18 mmol/L TeO_2 plus 3 mol/L HNO_3 (dashed),
25 mmol/L $Bi(NO_3)_3$ plus 5 mmol/L TeO_2 plus 3 mol/L HNO_3 (solid) (*a*).
The evolution of CV in successive cycles at different reversal potentials of potential scan.
Inset shows the cycle in the range of Bi UPD and Bi_{ad} anodic oxidation (*b*).
$dE/dt = 50$ mV · s^{-1}. The current was normalized for geometric surface area

indicates the adsorption capacitance absence in the faradaic branch of equivalent electric circuit [30] in Pb UPD on Bi_2Te_3. In fact, our analysis of PDEIS spectra of Pb UPD on Bi_2Te_3 has revealed a Randles type equivalent circuit which is characteristic of significantly irreversible electrochemical adsorption. The inverse charge transfer resistance dependence on electrode potential derived for this underpotential deposition process from its potentiodynamic electrochemical impedance spectrum (fig. 7, *b*) shows a characteristic peak similar to those observed in other irreversible UPD processes.

The surface limited character of the UPD allows relating the UPD charge Q to real surface area A of the substrate [22]:

$$A = Q/q,$$

where q is the charge required to form the full adlayer on 1 cm^2 of a substrate. The UPD charge for Pb UPD on tellurium $q = 400$ μC · cm^{-2} [20]. This charge approximately corresponds to a reduction of a closely packed layer of Pb atoms. In principle, q may vary slightly with a change of the substrate but is assumed to be a constant for the same supporting material with variable morphology. In the investigations of surface roughness variation, the actual value of q is in fact not very important and can be assumed to be the same for Te and Bi_2Te_3 substrates in Pb UPD. The current in fig. 7, *a*, was normalized for real surface area with this assumption to provide the further evaluation of the variable electrode surface area at variable conditions of Bi_2Te_3 electrodeposition.

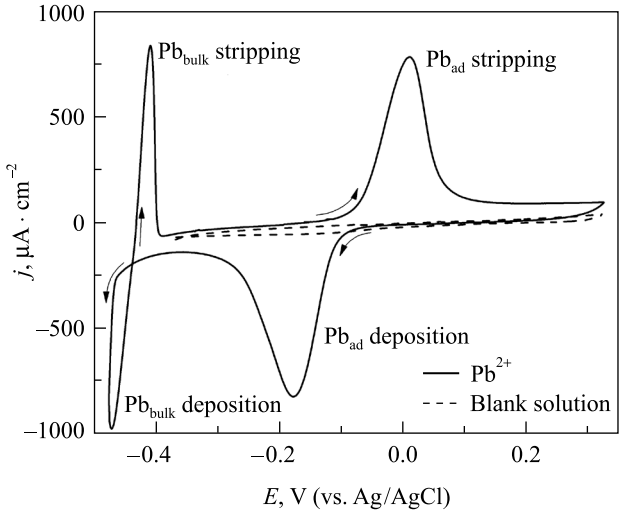

Fig. 6. Cyclic voltammogram of pulsed deposited Bi_2Te_3 electrode in 10 mmol/L $Pb(NO_3)_2$ plus 0.1 mol/L KNO_3 plus 10 mmol/L HNO_3 electrolyte solution (solid) and in blank 0.1 mol/L KNO_3 plus 10 mmol/L HNO_3 electrolyte (dashed). dE/dt = 50 mV · s^{-1}. The current was normalized for geometric surface area

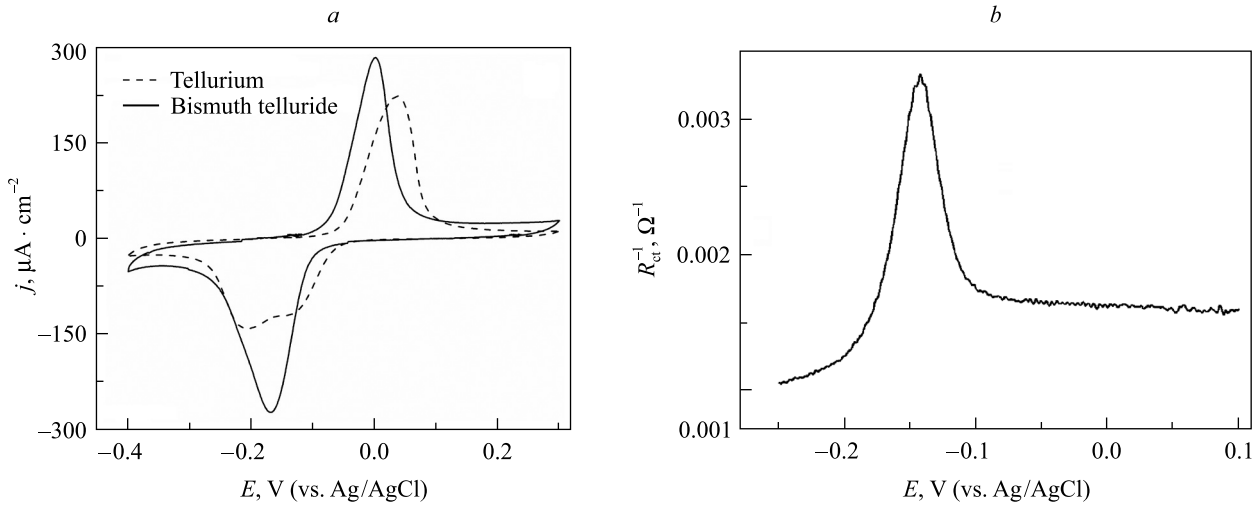

Fig. 7. Cyclic voltammograms of tellurium (dashed) and pulsed deposited Bi_2Te_3 (solid) electrodes at sustained cycling in the potential ranges of Pb UPD from 10 mmol/L $Pb(NO_3)_2$ plus 0.1 mol/L KNO_3 plus 10 mmol/L HNO_3 electrolyte solution. dE/dt = 50 mV · s^{-1}. The current was normalized for real surface area (*a*). Inverse charge transfer resistance of the UPD dependence on the potential (*b*)

Figure 8 compares Pb and Bi UPD on Bi_2Te_3 electrodeposits of different morphology. The solid curves in fig. 8 are potentiodynamic profiles of Bi UPD on Bi_2Te_3. The cathodic peak shows up 0.1 V above the starting potential of bulk bismuth electrodeposition. The latter proceeds below 0 V and the deposited metallic Bi gives the anodic peak far below the anodic peak of Bi adlayer on Bi_2Te_3 (fig. 8, *b*).

We make a note of the similarity of the part of the potentiodynamic profile which relates to Bi adlayer deposition and stripping and the CV in fig. 5, *b*, inset, which confirms the Bi UPD in the conditions of Bi_2Te_3 electrodeposition. Bismuth telluride deposits obtained by potential cycling with excess bismuth and by pulsed electrodeposition from «stoichiometric» solution give similar potentiodynamic profiles of Bi UPD, but the current and the corresponding UPD charge varies strongly with the electrodeposition condition, because of the variation of the real surface area (table). The explanation of the much higher roughness of the bismuth-rich deposit can be obtained from the potentiodynamic profiles of the electrodeposition shown in fig. 5, *b*.

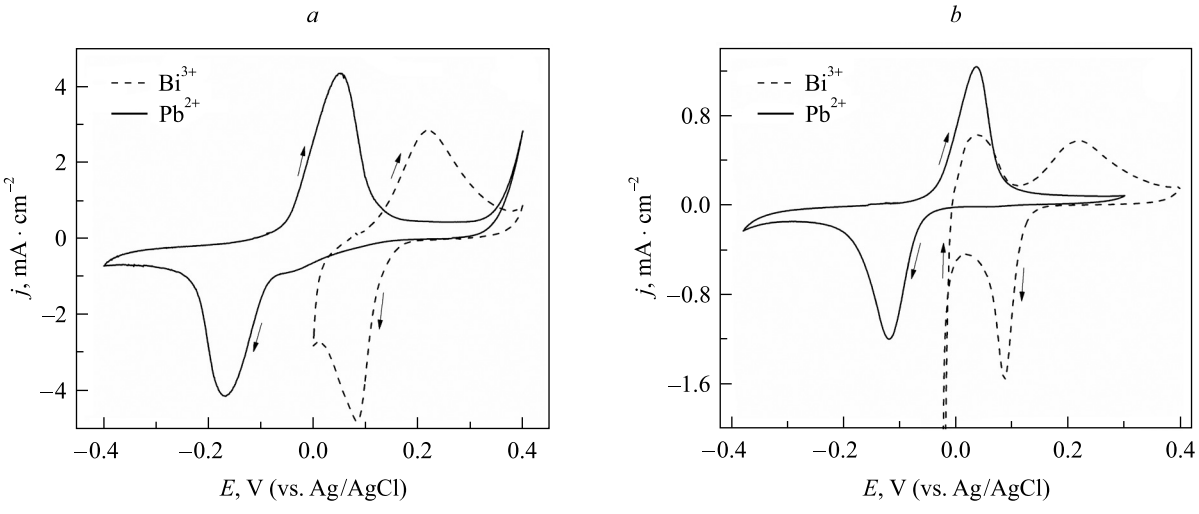

Fig. 8. Bi (dashed) and Pb (solid) UPD on Bi_2Te_3 electrodeposits prepared by different procedures:
a – potential cycling at d*E*/d*t* = 50 mV · s^{-1} (30 cycles) in the electrolyte
with Bi : Te = 5 : 1 (25 mmol/L $Bi(NO_3)_3$ plus 5 mmol/L TeO_2 plus 3mol/L HNO_3);
b – pulsed electrodeposited from «stoichiometric» electrolyte as described in the article.
Electrolytes: 25 mmol/L $Bi(NO_3)_3$ plus 3mol/L HNO_3 (Bi UPD),
10 mmol/L $Pb(NO_3)_2$ plus 10 mmol/L HNO_3 plus 0.1 mol/L KNO_3 (Pb UPD).
The current was normalized for geometric surface area. d*E*/d*t* = 50 mV · s^{-1}

Bismuth telluride surface area estimation

Deposition mode	Geometric area, mm^2	$q_{adlayer}$ [20], μC · cm^{-2}	$Q_{adlayer}$ stripping, μC	Real surface area, cm^2	Roughness factor
CV	20	400	1850	4.6	23.0
Pulses	24		450	1.1	4.7

The excessive bismuth which gives the anodic peak A_2 oxidizes above the potential of bulk metallic Bi though below the potential of Bi adlayer anodic oxidation. This type of Bi can correspond to Bi^0 intercalated in Van der Waals planes of Bi_2Te_3 crystal, where Bi – Bi_2Te_3 interaction should be relatively low. In fact, this «intercalated» bismuth is deposited during the electrodeposition of Bi_2Te_3. As the interactions in the Van der Waals planes are weak, this excessive bismuth produces no change of the chemical identity of the host material, therefore we observed no change in Bi UPD potential with the variation of the deposition conditions. The intercalation can be of interest as the means of loosening the interlayer interactions in the layered structure of bismuth telluride for its further application in exfoliation procedures.

Our results provide also some new insight into the mechanisms of bismuth telluride electrodeposition. We exclude any significant role of bulk bismuth in the sustained stage of Bi_2Te_3 electrodeposition in the potential range above the oxidation peak of bulk Bi typically used in the electrodeposition procedures. Bismuth adlayers contrary to bulk Bi, are much more resistant to anodic oxidation and their participation in Bi_2Te_3 crystal growth is very likely in the range of Bi UPD. The kinetic prevention of tellurium electrodeposition from Bi-free electrolyte on steel in the typical potential ranges of bismuth telluride electrodeposition should be not considered as a strong argument for elementary tellurium exclusion from electrodeposition mechanisms. Thermodynamically tellurium electrodeposition can proceed in this range and actually proceeds after overcoming the nucleation barrier. In view of Bi UPD similarity on Bi_2Te_3 and Te, those tellurium nuclei, if they are formed by induced codeposition, are expected to attract bismuth adatoms and thus be drawn into the telluride crystal growth. More likely for this reason, rather than because of tellurium deposition prevention, Bi_2Te_3 electrodeposits can be obtained free of tellurium inclusions.

Conclusion

The UPD of metals on chalcogenides is of great interest as a means of the electrochemical surface characterization. The UPD processes of lead and bismuth on bismuth telluride (Bi_2Te_3) have been discovered with the underpotential shifts 0.3 V for Pb UPD and 0.1 V for Bi UPD. The Pb UPD was shown to be helpful for bismuth telluride real surface area evaluation. Pb UPD proceeds significantly different on bismuth telluride and tellurium substrates, which helps to control purity of bismuth telluride electrodeposit.

In order to study Pb and Bi UPD, bismuth telluride films were deposited from acidic solution of TeO_2 and bismuth salt on steel substrates using potential pulse electrodeposition and cyclic voltammetry. The CV has proved that the stoichiometric bismuth telluride electrodeposition proceeds in the potential range of metallic bismuth anodic oxidation which excludes metallic Bi as a required intermediate in the sustained electrodeposition of Bi_2Te_3. Bismuth adatoms are much more stable than metallic Bi on Bi_2Te_3 and they are very likely to be involved in the electrodeposition mechanisms at potentials above $E(Bi^{3+}/Bi^0_{bulk})$. The potentials of pulsed electrodeposition were optimized using the information on Bi UPD. The electrodeposited Bi_2Te_3 purity from Te and Bi phases was proved by XRD and potentiodynamic profile of Pb UPD.

The Bi_2Te_3 electrodeposition from electrolyte with significant excess of Bi^{3+} over TeO_2 can proceed with formation of the Bi^0 form with oxidation potential intermediate between those of metallic Bi and Bi adlayer that was attributed to Bi atoms intercalated in Van der Waals planes of bismuth telluride. The effect of Bi intercalation is of interest as a means of loosening the interlayer interactions in the layered structure of bismuth telluride for its further application in exfoliation procedures.

References

1. Eibl O., Nielsch K., Peranio N., et al. (eds). Thermoelectric Bi_2Te_3 Nanomaterials. Weinheim, 2015. DOI: 10.1002/9783527672608.

2. Biswas K., He J., Blum I. D., et al. High-performance bulk thermoelectrics with all-scale hierarchical architectures. *Nature.* 2012. Vol. 489, issue 7416. P. 414–418. DOI: 10.1038/nature11439.

3. Richoux V., Diliberto S., Boulanger C., et al. Pulsed electrodeposition of bismuth telluride films: influence of pulse parameters over nucleation and morphology. *Electrochimica Acta*. 2007. Vol. 52, issue 9. P. 3053–3060. DOI: 10.10.16/j.electacta.2006.09.042.

4. Lei C., Ryder K. S., Koukharenko E., et al. Electrochemical deposition of bismuth telluride thick layers onto nickel. *Electrochem. Commun.* 2016. Vol. 66. P. 1–4. DOI: 10.1016/j.elecom.2016.02.005.

5. Gregory B. W., Stickney J. L. Electrochemical atomic layer epitaxy (ECALE). *J. Electroanal. Chem. Interfacial Electrochem.* 1991. Vol. 300, issue 1–2. P. 543–561. DOI: 10.1016/0022-0728(91)85415-L.

6. Bondarenko A. S., Ragoisha G. A., Osipovich N. P., et al. Potentiodynamic electrochemical impedance spectroscopy of lead UPD on polycrystalline gold and on selenium atomic underlayer. *Electrochem. Commun.* 2005. Vol. 7, No. 6. P. 631–636. DOI: 10.1016/j.elecom.2005.04.001.

7. Bondarenko A. S., Ragoisha G. A., Osipovich N. P., et al. Multiparametric electrochemical characterisation of Te – Cu – Pb atomic three-layer structure deposition on polycrystalline gold. *Electrochem. Commun*. 2006. Vol. 8, No. 6. P. 921–926. DOI: 10.1016/j.elecom.2006.03.033.

8. Chulkin P. V., Aniskevich Y. M., Streltsov E. A., et al. Underpotential shift in electrodeposition of metal adlayer on tellurium and the free energy of metal telluride formation. *J. Solid State Electrochem*. 2015. Vol. 19, No. 9. P. 2511–2516. DOI: 10.1007/s10008-015-2831-x.

9. Ivanou D. K., Ivanova Y. A., Ragoisha G. A., et al. Electrodeposition of tellurium and on tellurium. In: Grey D. (ed.). *Tellurium: Properties, Uses Research.* New York, 2017.

10. Hicks L. D., Dresselhaus M. S. Effect of quantum-well structures on the thermoelectric figure of merit. *Phys. Rev. B*. 1993. Vol. 47, No. 19. P. 12727–12731. DOI: 10.1103/PhysRevB.47.12727.

11. Wang G., Zhu X. G., Sun Y. Y., et al. Topological insulator thin films of Bi_2Te_3 with controlled electronic structure. *Adv. Mater*. 2011. Vol. 23, No. 26. P. 2929–2932. DOI: 10.1002/adma.201100678.

12. Fornari C. I., Rappl P. H., Morelhão S. L., et al. Structural properties of Bi_2Te_3 Topological insulator thin films grown by molecular beam epitaxy on (111) BaF_2 substrates. *J. Appl. Phys*. 2016. Vol. 119, No. 16. P. 165303. DOI: 10.1063/1.4947266.

13. Clavilier J., Feliu J. M., Aldaz A. An irreversible structure sensitive adsorption step in bismuth underpotential deposition at platinum electrodes. *J. Electroanal. Chem. Interfacial Electrochem.* 1988. Vol. 243, No. 2. P. 419–433. DOI: 10.1016/0022-0728(88)80045-7.

14. Sayed S. M., Jüttner K. Electrocatalysis of oxygen and hydrogen peroxide reduction by UPD of bismuth on poly- and mono-crystalline gold electrodes in acid solutions. *Electrochimica Acta*. 1983. Vol. 28, No. 11. P. 1635–1641. DOI: 10.1016/0013-4686(83)85228-1.

15. Ragoisha G. A., Bondarenko A. S. Potentiodynamic electrochemical impedance spectroscopy. *Electrochimica Acta*. 2005. Vol. 50, No. 7. P. 1553–1563. DOI: 10.1016/j.electacta.2004.10.055.

16. Zhu W., Yang J. Y., Gao X. H., et al. The underpotential deposition of bismuth and tellurium on cold rolled silver substrate by ECALE. *Electrochimica Acta*. 2005. Vol. 50, No. 27. P. 5465–5472. DOI: 10.1016/j.electacta.2005.03.028.

17. Gregory B. W., Norton M. L., Stickney J. L. Thin-layer electrochemical studies of the underpotential deposition of cadmium and tellurium on polycrystalline Au, Pt and Cu electrodes. *J. Electroanal. Chem. Interfacial Electrochem*. 1990. Vol. 293, No. 1. P. 85–101. DOI: 10.1016/0022-0728(90)80054-A.

18. Ragoisha G. A., Bondarenko A. S., Osipovich N. P., et al. Multiparametric characterisation of metal-chalcogen atomic multilayer assembly by potentiodynamic electrochemical impedance spectroscopy. *Electrochimica Acta*. 2008. Vol. 53, No. 11. P. 3879–3888. DOI: 10.1016/j.electacta.2007.09.017.

19. Osipovich N. P., Streltsov E. A., Susha A. S. Bismuth underpotential deposition on tellurium. *Electrochem. Commun*. 2000. Vol. 2, No. 12. P. 822–826. DOI: 10.1016/s1388-2481(00)00130-2.

20. Ragoisha G. A., Bondarenko A. S., Osipovich N. P., et al. Potentiodynamic electrochemical impedance spectroscopy: lead underpotential deposition on tellurium. *J. Electroanal. Chem*. 2004. Vol. 565, No. 2. P. 227–234. DOI: 10.1016/j.jelechem.2003.10.014.

21. Harman T. C., Walsh M. P., Laforge B. E., et al. Nanostructured thermoelectric materials. *J. Electron. Mater.* 2005. Vol. 34, No. 5. P. 19–22. DOI: 10.1007/s11664-005-0083-8.

22. Trasatti S., Petrii O. A. Real surface area measurements in electrochemistry. *J. Electroanal. Chem*. 1992. Vol. 327, issue 1–2. P. 353–376. DOI: 10.1016/0022-0728(92)80162-w.

23. Malashchonak M. V., Streltsov E. A., Ragoisha G. A., et al. Evaluation of electroactive surface area of CdSe nanoparticles on wide bandgap oxides (TiO_2, ZnO) by cadmium underpotential deposition. *Electrochem. Commun*. 2016. Vol. 72. P. 176–180. DOI: 10.1016/j.elecom.2016.10.004.

24. Zheng J., Zhang H., Dong S., et al. High yield exfoliation of two-dimensional chalcogenides using sodium naphthalenide. *Nature Commun.* 2014. Vol. 5, Article number 2995. DOI: 10.1038/ncomms3995.

25. Soriaga M. P., Stickney J., Bottomley L. A., et al. Thin Films: Preparation, Characterization, Applications. New York, 2012. DOI: 10.1007/978-1-4615-0775-8.

26. Nicolosi V., Chhowalla M., Kanatzidis M. G., et al. Liquid exfoliation of layered materials. *Science*. 2013. Vol. 340, No. 6139, Article number 1226419. DOI: 10.1126/science.1226419.

27. Ma Y., Johansson A., Ahlberg E., et al. A mechanistic study of electrodeposition of bismuth telluride on stainless steel substrates. *Electrochimica Acta*. 2010. Vol. 55, No. 15. P. 4610–4617. DOI: 10.1016/j.electacta.2010.03.018.

28. Ragoisha G. A., Bondarenko A. S. Potentiodynamic electrochemical impedance spectroscopy for solid state chemistry. *Solid State Phenomena*. 2003. Vol. 90–91. P. 103–108. DOI: 10.4028/www.scientific.net/SSP.90-91.103.

29. Bondarenko A. S., Ragoisha G. A. Progress in Chemometrics Research. New York, 2005. P. 89–102.

30. Ragoisha G. A. Potentiodynamic electrochemical impedance spectroscopy for underpotential deposition processes. *Electroanalysis*. 2015. Vol. 27, No. 4. P. 855–863. DOI: 10.1002/elan.201400648.

31. Chichagov A. V., Belonozhko A. B., Lopatin A. L., et al. The information processing system on crystal structures of minerals (Mincryst). *Kristallografiya.* 1990. Vol. 35, No. 3. P. 610–616.

Received by editorial board 13.02.2017.